System Concepts for Bi- and Multi-Static SAR Missions

Gerhard Krieger, Hauke Fiedler, Marc Rodriguez-Cassola, David Hounam, and Alberto Moreira
Institut für Hochfrequenztechnik und Radarsysteme
Deutsches Zentrum für Luft- und Raumfahrt (DLR)
82234 Oberpfaffenhofen, Germany
Tel.: +49 8153 28 3054, E-Mail: Gerhard.Krieger@dlr.de

Abstract

The performance and capabilities of bi- and multistatic spaceborne synthetic aperture radar (SAR) are analyzed. Such systems can be optimized for a broad range of applications like frequent monitoring, wide swath imaging, single-pass cross-track interferometry, along-track interferometry, resolution enhancement or radar tomography. Further potentials arises from digital beamforming on receive, which allows to gather additional information about the direction of the scattered radar echoes. This directional information can be used to suppress interferences, to improve geometric and radiometric resolution, or to increase the unambiguous swath width. Furthermore, a coherent combination of multiple receiver signals will allow for a suppression of azimuth ambiguities. For this, a reconstruction algorithm is derived, which enables a recovery of the unambiguous Doppler spectrum also in case of non-optimum receiver aperture displacements leading to a non-uniform sampling of the SAR signal. This algorithm has also a great potential for systems relying on the displaced phase center (DPC) technique, like the high resolution wide swath (HRWS) SAR or the split antenna approach in the TerraSAR-X and Radarsat II satellites.

1. INTRODUCTION

Bi- and multistatic synthetic aperture radar (SAR) operates with individual transmit and receive antennas which are mounted on separate platforms. Such a spatial separation has several operational advantages which will increase the capability, reliability and flexibility of future SAR missions. The transmitter and receiver satellites may be in low earth orbit (LEO), medium earth orbit (MEO), or geosynchronous orbit (GEO) and the whole satellite constellation can be optimized for different applications which require frequent monitoring and/or wide swath imaging. Figure 1 shows an example for a spaceborne constellation which combines a geostationary transmitter with multiple passive receivers in low earth orbit (see also [1]-[4]). This specific combination has the potential to provide a cost-effective solution to the frequent monitoring problem, since only low-cost receivers with small antennas have to be duplicated to shorten the revisit times. The active illuminator can also be combined with multiple passive receivers flying in close formation. This will yield a multistatic SAR, which enables a broad range of powerful remote sensing applications. Examples are single-pass cross-track interferometry for the generation of highly accurate digital elevation models (DEMs), sparse aperture constellations for moving target indication and large area traffic monitoring, along-track interferometry for the mapping of ocean currents and ice drift, bistatic scattering for improved scene classification, and polarimetric interferometry or even tomography for 3-D vegetation mapping (cf. [5]-[9]). All these applications may share one or a small number of common illuminators, thereby reducing the individual costs of each mission substantially.

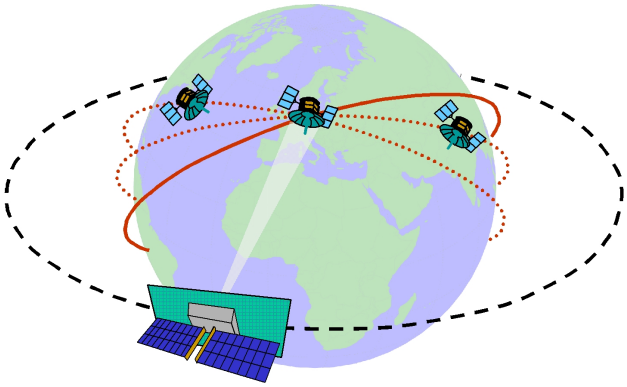

Figure 1: Geostationary illuminator with LEO receivers

2. PERFORMANCE ANALYSIS FOR BISTATIC SAR SYSTEMS

In this section, the performance of the bistatic configuration shown in Figure 1 will be investigated. Since the following analysis takes full account of the bistatic imaging geometry, it is also applicable to other bistatic SAR constellations, like a global earth observation system with continuous monitoring based on multiple MEO satellites. The major parameters of an exemplary bistatic system are summarized in Table I.

TABLE I. SYSTEM PARAMETERS FOR A BISTATIC SAR WITH GEOSTATIONARY ILLUMINATOR AND LEO RECEIVERS

Wavelength	λ	3.1 cm (X-Band)
Max. Bandwidth	B_r	300 MHz
Average Transmit Power	P_t	1000 W
Antenna Size Tx	A_{Tx}	100 m^2
Antenna Size Rx	A_{Rx}	6 m^2
Noise Figure + Losses	$F+L$	5dB
Transmitter Altitude	h_{Tx}	35850 km (geostat.)
Receiver Altitude	h_{Rx}	400 km
Inclination (Receiver Orbit)	i	50°
Ground Range Resolution	Δrg	3 m
Azimuth Resolution	Δaz	3 m

In order to simplify the analysis, all computations will be performed in a local plane *(x,y)* which is tangent to the earth's surface at the receiver nadir. The errors introduced by this approximation may be neglected for small receiver altitudes and it would be straightforward to extend the results to a spherical or elliptical geometry for receivers in higher orbits.

We start with a closer look at the resolution cell of the bistatic SAR. Figure 2 shows the contours with constant range and Doppler in the tangent plane *(x,y)* for a receiver at *50°* latitude and the same longitude as the geostationary transmitter. The circle in the center denotes the receiver nadir and the arrow indicates the receiver velocity. Since there is a priori no obvious range direction in a bistatic SAR, we define the range resolution vector field $\vec{r}_g$ in the tangent plane *(x,y)*

$$\vec{r}_g(x,y) = \frac{\operatorname{grad}[r(x,y)]}{\left\|\operatorname{grad}[r(x,y)]\right\|^2} \cdot \frac{c_0}{B_r}$$

where $r(x,y) = r_{Tx}(x,y) + r_{Rx}(x,y)$ is the sum of the transmit and receive range in the tangent plane, c_0 is the speed of light and B_r is the bandwidth of the transmitted signal. Note that for each position in the tangent plane the vector $\vec{a}_g$ points always in the direction of the best range resolution (as is true for the ground range in a monostatic SAR) and its length indicates the achievable ground range resolution. In a similar manner we may derive the Doppler resolution vector

$$\vec{a}_g(x,y) = \frac{\operatorname{grad}\left[f_{Dop}(x,y)\right]}{\left\|\operatorname{grad}\left[f_{Dop}(x,y)\right]\right\|^2} \cdot \frac{1}{T_{\text{int}}(x,y)}$$

where T_{int} denotes the receiver's coherent integration time and

$$f_{Dop} = -\frac{1}{\lambda}\left[\frac{\partial}{\partial t}\left(r_{Tx} + r_{Rx}\right)\right] = -\frac{1}{\lambda}\left[\frac{\partial r_{Tx}}{\partial t} + \frac{\partial r_{Rx}}{\partial t}\right]$$

is the Doppler frequency of the bistatic SAR. Note that for the present system $\partial r_{Tx}/\partial t = 0$ which will reduce the Doppler frequency and increase the SNR by a factor of two if compared to a monostatic SAR. Based on these definitions we may

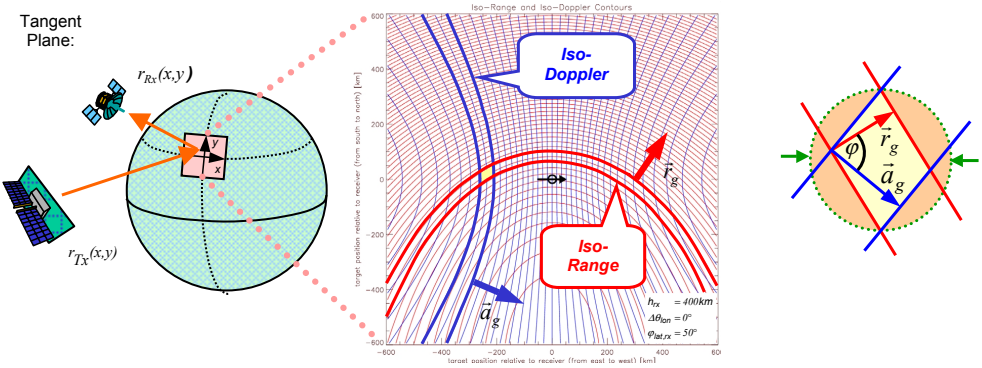

Figure 2: Left: Iso-Range (red) and Iso-Doppler (blue) Contours. Right: Resolution cell of a bistatic SAR

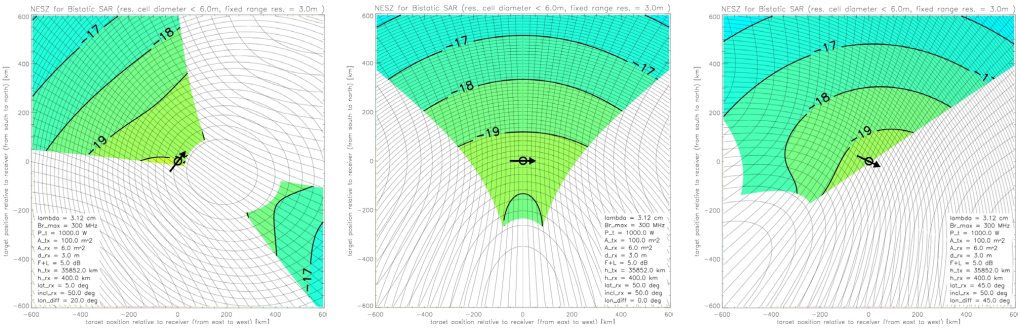

Figure 3: NESZ in tangential plane for receiver satellites at different longitudes and latitudes. Latitudes of the receiver are 5° (left), 50° (middle) and 45° (right) and longitude differences between transmitter and receiver are 20° (left), 0° (middle), and 45° (right).

derive the area of a bistatic resolution cell (cf. Figure 2, right) as

$$A_{rescell} = \frac{\left\|\vec{r}_g\right\| \cdot \left\|\vec{a}_g\right\|}{\sin(\varphi)} = \frac{\left\|\vec{r}_g\right\|^2 \cdot \left\|\vec{a}_g\right\|^2}{\left\|\vec{r}_g \times \vec{a}_g\right\|}$$

where φ is the angle between the range and azimuth resolution vectors $\vec{r}_g$ and $\vec{a}_g$. For a calculation of the sensitivity of the system we start from the bistatic radar equation (cf. [10])

$$SNR = \frac{P_t G_{Tx}}{4\pi r_{Tx}^2} \cdot A_{rescell} \sigma_B^0 \cdot \frac{A_{Rx}}{4\pi r_{Rx}^2} \cdot \frac{1}{kT_S F B_{noise} L},$$

where P_t is the average transmit power, G_{Tx} the gain of the transmitting antenna, $A_{rescell}$ the size of the resolution cell for one look, A_{Rx} the effective aperture of the receive antenna, r_{Tx} the slant range distance from the transmitter to the imaged scene, r_{Rx} the slant range distance from the receiver to the imaged scene, k the Boltzmann constant, T_S the system noise temperature, F the noise figure, B_{noise} the effective noise bandwidth, and L the loss factor. As the noise equivalent sigma zero (*NESZ)* corresponds to the radar scattering coefficient σ_B^0 for which the signal-to-noise ratio is equal to one, we get after a simple transformation

$$NESZ = \frac{(4\pi)^2 r_{Tx}^2 r_{Rx}^2 k T_s F L}{P_t G_{Tx} A_{Rx} \cdot A_{rescell} \cdot T_{\text{int}}}$$

where we assumed that after coherent integration in range and azimuth the effective noise bandwidth is given by $B_{noise} = 1/T_{\text{int}}$. Figure 3 shows the *NESZ* for three different receiver locations. In the *NESZ* computation we assumed a fixed ground range resolution of *3m* which requires a position dependent range bandwidth B_r (e.g. *125MHz* at receiver nadir). Since the bandwidth may not exceed an upper limit of *300MHz*, we have restricted the *NESZ* computation to those areas where B_r<*300MHz*. In Figure 3 we have further assumed that the diameter of the resolution cell $d_{rescell}$, which is shown dotted in Figure 2 on the right, does not exceed a predefined limit of *6m* for an azimuth resolution of *3m*. The resolution cell diameter can be derived from the range and azimuth resolution vectors by

$$d_{rescell} = \frac{\sqrt{\left\|\vec{r}_g\right\|^2 + \left\|\vec{a}_g\right\|^2 + 2 \cdot \left\|\vec{r}_g\right\| \cdot \left\|\vec{a}_g\right\| \cdot \left|\cos(\varphi)\right|}}{\left|\sin(\varphi)\right|}$$

From Figure 3 it becomes clear that the *NESZ* for the configuration of Table I will be in the order of *-19dB* for targets in the neighborhood of the receiver nadir. In this context it is interesting to note that – in contrast to a monostatic SAR – we may achieve a good ground resolution in all directions of the passive receiver nadir, i.e., high resolution SAR imaging is also possible in the forward, downward and backward direction of the moving receiver. This property increases the access region and may also open new application areas like a data fusion with simultaneously acquired data from different downward-looking sensors (e.g. optical, altimeter, etc.) on the same platform. Another promising application is a high resolution forward-looking radar for airborne systems, where one or several stationary transmitters either on the ground or in space are combined with a passive SAR receiver on the aircraft.

3. DIGITAL BEAMFORMING IN BI- AND MULTISTATIC SAR

The system of Table I has the interesting peculiarity that the transmit path exceeds by far the distance from the target to the receiver. As a result of the long transmit path, the antenna footprint of the geostationary illuminator will have an extension of more than hundred kilometers in both azimuth and range. This is in fundamental contrast to the small

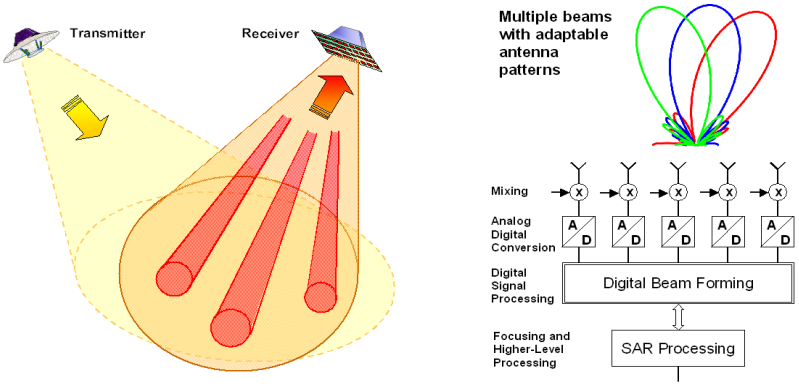

Figure 4: Digital beamforming on receive

footprints of the LEO receivers for which we will have a typical diameter in the order of 6 km assuming a downward-looking parabolic antenna with a radius of 1.25m. Thus, the simultaneously accessible region with a fixed aperture receiver is very limited. Such a limitation may be avoided by digital beamforming (DBF) on receive, where the receiver antenna is split into multiple sub-apertures and each sub-aperture signal is separately amplified, down-converted, and digitized (cf. Figure 4, right). The digital signals can then be combined in a dedicated signal processor to form multiple antenna beams with arbitrary shapes. This makes effective use of the total signal energy within the large illuminated footprint and will introduce a high flexibility in operating the bistatic SAR constellation.

Digital Beamforming in Elevation: The formation of multiple independent beams in elevation allows for the simultaneous mapping of several distinct subswaths with full azimuth resolution and high antenna gain. By combining multiple subswaths, it is also possible to map a wide image swath (>100km). Furthermore, the use of a frequency modulated continuous wave (FMCW) illumination source with low chirp rate will allow for a sub-sampling of the recorded signals, thereby reducing the data rate substantially. This is due to the fact, that at any instant of time the bandwidth within a sufficiently narrow elevation beam will only be a small fraction of the total bandwidth of the transmitted chirp (cf. Figure 5, left). The digital beamforming corresponds therefore to a bandpass filter bank which divides the recorded range spectrum in multiple sub-spectra. The time-variant shift of the center frequency within each beam can easily be removed either by dechirp on receive or, more conveniently, in the final SAR processing. The problem of selecting optimum DBF coefficients and appropriate sub-sampling rates for each channel may be treated in the more general framework of multi-channel digital signal processing in combination with rate distortion theory. Note that in case of short transmit pulses it is also possible to restrict the length of the receiving window of each DBF channel on the cost of an increased sub-sampling frequency. The optimization of such a system may be regarded as the problem of optimum bit-allocation in a 3-D information cube, where the three axes correspond to time, frequency, and spatial direction of the recorded signals (cf. Figure 5, right).

Digital Beamforming in Azimuth: The formation of multiple beams in azimuth will allow for the division of a broad Doppler spectrum into multiple sub-spectra with different Doppler centroids. The bandwidth in each subchannel corresponds to the total length of the receiver antenna, which determines the minimum allowable PRF. A coherent combination of the sub-spectra will then yield a broad Doppler bandwidth for high azimuth resolution. This technique is especially attractive for high resolution imaging with SAR systems that require long antenna structures for the unambiguous imaging of a wide swath. The formation of multiple beams in azimuth is also an interesting alternative to the displaced phase center (DPC) technique in [12]. Note that the suggested Doppler frequency splitting is functionally equivalent to a spotlight-on receive SAR where the beamsteering can be regarded as a temporal scanning of different DBF channels in azimuth. Therefore, the sensitivity of the complete system will be comparable to that of a spotlight-on receive SAR (cf. [15]), while the final image will span the complete area illuminated by the transmitter. The high azimuth resolution in case of large illuminated footprints can also be used to improve the signal-to-noise ratio or the radiometric resolution of the whole system.

Interference and Ambiguity Suppression: Digital beamforming allows for a minimization of any performance degradation due to an interference with transmit and/or nadir signals. This is of special interest, if continuous recording is used to obtain a wide image swath. To avoid a possible saturation of the low noise amplifier and the subsequent A/D converters in the receiver, it is preferred to use long transmit pulses or even continuous wave illumination (CW). This will also reduce the peak power requirements in the transmitter. Furthermore, digital beamforming on receive will allow for the efficient suppression of range and azimuth ambiguities by inserting appropriate nulls in the antenna pattern. Null-steering in elevation [13] may be used to suppress range ambiguities within the illuminated swath. Hence, the unambiguous swath width is no longer restricted by the PRF and the opportunity to increase the PRF during wide swath imaging will contribute to the development of more compact SAR sensors with reduced antenna length and increased antenna height. This avoids a complicated antenna folding during satellite launch.

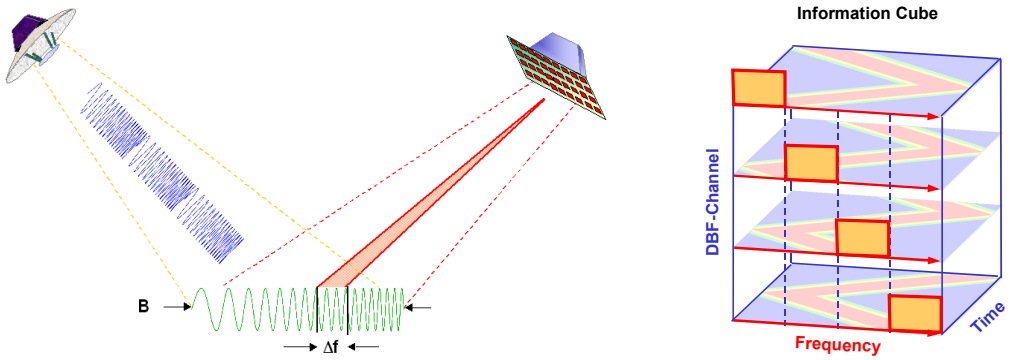

Figure 5: Bandwidth limitation by digital beamforming on receive in a bistatic frequency modulated continuous wave radar (FMCW).

4. MULTIPLE APERTURE SAMPLING IN ALONG-TRACK

The use of multiple receiver apertures in combination with a large azimuth footprint allows also for a reduction of the PRF, thereby increasing the non-ambiguous swath width. The apertures may be either on a single platform like in the Displaced Phase Center (DPC) antenna technique ([12]-[15]) or on different platforms ([16][17]) leading to a multistatic SAR where the size of each individual receiver is reduced. One example for such a scenario is shown in Figure 6 on the left, where a single transmitter illuminates a wide swath and n receivers record simultaneously the scattered signal from the illuminated footprint. Under ideal conditions, this will allow for a reduction of the PRF by a factor of n without raising azimuth ambiguities. This reduction of the azimuth sampling rate becomes possible by a coherent combination of the individual receiver signals where the ambiguous parts of the Doppler spectra cancel each other. For optimum performance, the along-track distance of the passive receivers ($i = \{2,3,...,n\}$) relative to the first receiver ($i = 1$) should be selected as

$$x_i - x_1 \approx \frac{2v}{PRF}\left(\frac{i-1}{n} + k_i\right) \qquad k_i \in Z \tag{1}$$

but, as we will see later, an unambiguous recovery of the Doppler spectrum is also possible for other distances as long as the virtual samples of the azimuth signal do not coincide. Note that the selection of different k_i for each satellite gives a great flexibility in choosing the along-track distance between the receivers. Equation (1) includes also the classic DPC approach in [12][13][14] as well as the split antenna techniques for Radarsat II and TerraSAR-X as special cases where we have $k_i = 0$. For $n=2$, a possible variation in the along-track distance can also be compensated by an appropriate adaptation of the PRF, thereby avoiding the necessity of precise orbit control in case of a multistatic satellite constellation. In this context it is also important to note that the PRF may not be adapted arbitrarily as long as the transmitter and receiver are on the same platform, since such a system will not allow for simultaneous transmission and reception. This restriction will also apply to the split antennas in Radarsat II and TerraSAR-X [18][19].

In the following we will show that an unambiguous recovery of the Doppler spectrum is also possible in case of a deviation from the optimum-sampling displacement given in equation (1). For this, we consider a multiple aperture SAR as a linear system with multiple receiver channels (cf. Figure 6, right). For such a system, there exist a lot of powerful theorems in linear systems theory. Of special importance for the present context is a generalization of the sampling theorem according to which a band-limited signal $u(t)$ is uniquely determined in terms of the samples $h_i(nT)$ of the responses $h_i(t)$ of n linear systems with input $u(t)$, sampled at $1/n$ of the Nyquist frequency [20]. In order to be valid, the transfer functions of the linear filters may be selected in a quite general sense, but not arbitrarily (for details, see [20] and [21]). The original derivation of this result uses a linear system of time and frequency varying equations for the reconstruction of the signal $u(t)$ from the samples $h_i(nT)$ [20]. A more elegant approach has been derived by J.L. Brown in [21] based on a minimum error energy criterion. A block diagram for the reconstruction from the subsampled signals is shown in Figure 7. As can be seen from Figure 7 on the left, the reconstruction consists essentially of n linear filters $P_i(f)$ which are individually applied to the sub-sampled signals of the receiver channels and then superimposed. As shown in Figure 7 on the right, each of the reconstruction filters $P_i(f)$ can again be regarded as a composition of n bandpass filters $P_{ij}(f)$, where $1 \le j \le n$. In [21], it has been shown that the transfer functions can be derived from a matrix $\mathbf{H(f)}$ which consists of the n transfer functions $H_i(f)$ which have to be shifted by integer multiples of the PRF in the frequency domain:

$$\mathbf{H(f)} = \begin{bmatrix} H_1(f) & H_2(f) & \cdots & H_n(f) \\ H_1(f+PRF) & H_2(f+PRF) & \cdots & H_n(f+PRF) \\ \vdots & \vdots & \ddots & \vdots \\ H_1(f+(n-1)\cdot PRF) & H_2(f+(n-1)\cdot PRF) & \cdots & H_n(f+(n-1)\cdot PRF) \end{bmatrix} \tag{2}$$

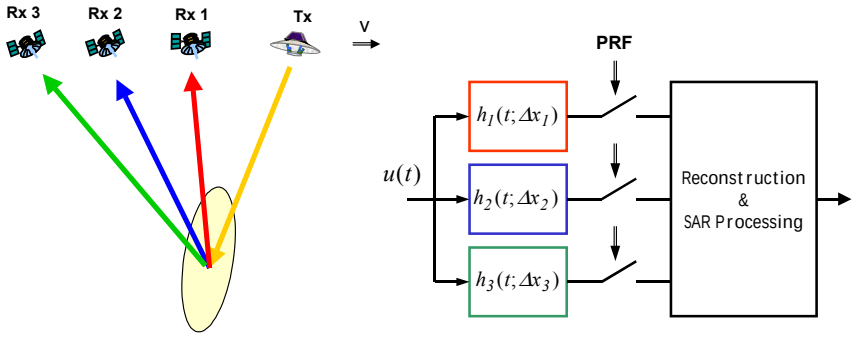

Figure 6: Multistatic SAR for Wide Swath Imaging with Small Antennas. Left: Satellite constellation. Right: Linear system model

The reconstruction filters $P_{ij}(f)$ are then derived from a matrix inversion of $\mathbf{H(f)}$ as

$$\mathbf{H}^{-1}(\mathbf{f}) = \begin{bmatrix} P_{11}(f) & P_{12}(f+PRF) & \cdots & P_{1n}(f+(n-1)PRF) \\ P_{21}(f) & P_{22}(f+PRF) & \cdots & P_{2n}(f+(n-1)PRF) \\ \vdots & \vdots & \ddots & \vdots \\ P_{n1}(f) & P_{n2}(f+PRF) & \cdots & P_{nn}(f+(n-1)PRF) \end{bmatrix} \quad (3)$$

In principle, it is possible to use the multi-channel SAR signal model for a complete reconstruction of the scene reflectivity. However, in order to concentrate on the essential steps, we will only consider the azimuth modulation in the following derivation. The azimuth signal of a point target at azimuth time $t = 0$ and slant range r_0 for each individual receiver channel i may be described as

$$h_i(t;\Delta x_i) = A_{Tx}(vt)\cdot A_{Rx,i}(vt)\cdot \exp\left[-j\frac{2\pi}{\lambda}\left(\sqrt{r_0^2+(vt)^2}+\sqrt{r_0^2+(vt-\Delta x_i)^2}\right)\right] \quad (4)$$

where A_{Tx} and $A_{Rx,i}$ define the envelope of the azimuth signal arising from the projection of the transmit and receive antenna patterns on the ground. The phase of the azimuth signal is proportional to the sum of the transmit and receive paths which are here approximated by the two square roots assuming a straight flight path with velocity v. A further simplification arises if we expand (4) in a Taylor series up to the second order which will lead to the quadratic approximation:

$$h_i(t;\Delta x_i) \cong A_{Tx}(vt)\cdot A_{Rx,i}(vt)\cdot \exp\left[-j\frac{4\pi}{\lambda}r_0\right]\cdot \exp\left[-j\frac{\pi\Delta x_i^2}{2\lambda r_0}\right]\cdot \exp\left[-j\frac{2\pi v^2}{\lambda}\frac{\left(t-\frac{\Delta x_i}{2v}\right)^2}{r_0}\right] \quad (5)$$

Here, the first exponential describes a constant phase offset for a given slant range r_0 which is equal for all receivers while the second exponential accounts for an additional constant phase offset which is due to the different along-track displacements between each individual receiver and the transmitter. The time-varying azimuth modulation of the bistatic SAR is then given by the third exponential. By comparing (5) with the point target response of a monostatic SAR

$$h_i(t;\Delta x_i) \cong \tilde{A}_{Tx}(vt)\cdot \tilde{A}_{Rx}(vt)\cdot \exp\left[-j\frac{4\pi}{\lambda}r_0\right]\cdot \exp\left[-j\frac{2\pi v^2 t^2}{\lambda r_0}\right] \quad (6)$$

it becomes clear that the bistatic azimuth response evolves from its monostatic counterpart by a time delay $\Delta t = \Delta x_i/2v$ and a phase shift $\Delta\varphi = -\pi\Delta x_i^2/2\lambda r_0$ if we substitute the antenna footprints A_{Tx} and A_{Rx} by $\tilde{A}_{Tx}(vt) = A_{Tx}(vt+\Delta x_i/2)$ and $\tilde{A}_{Rx}(vt) = A_{Rx}(vt+\Delta x_i/2)$. The bistatic antenna footprint is then given by

$$A_i(vt) = \tilde{A}_{Tx}(vt)\cdot \tilde{A}_{Rx}(vt) = A_{Tx}\left(vt+\frac{\Delta x_i}{2}\right)\cdot A_{Rx}\left(vt+\frac{\Delta x_i}{2}\right)$$

Therefore, the multiple aperture system can be regarded as a monostatic SAR which is followed by additional time and phase shifts for each receiver channel. This is illustrated in Figure 8. Since the joint antenna footprint may be different for each receiver, we have also introduced a separate amplitude weighting of the azimuth spectrum in each channel, but it is also possible to separate the joint antenna pattern in two parts where a first weighting function in the monostatic SAR response accounts for a weighting of the Doppler spectrum which is common to all receivers and the second transfer function in each channel accounts for residual deviations between the individual receivers. These deviations may for

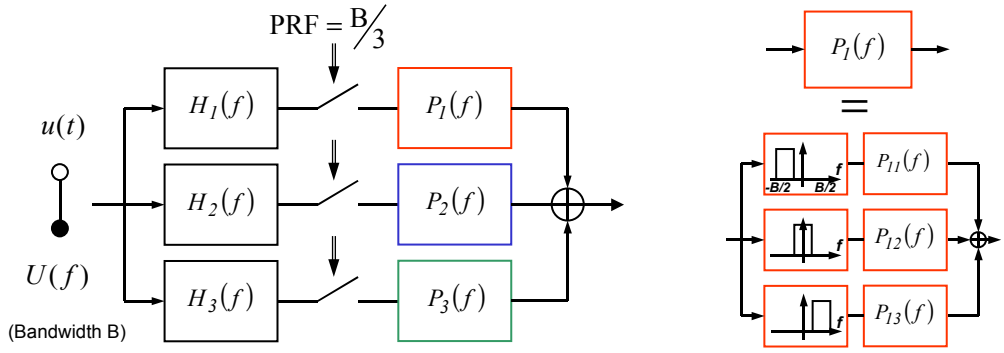

Figure 7: Reconstruction for multi-channel subsampling in case of three channels.

example result from different Doppler centroids due to the different along-track displacements, inaccuracies in the antenna pointing, or a mutual coupling between the antenna sub-arrays in case of DPC based on a single platform. It may be expected, that such a separation in two transfer functions will have an impact on the stability of the signal reconstruction, but this topic deserves further investigation.

Analytic example for two receivers:

As a simple example for an analytic derivation of the reconstruction filters we consider a bistatic SAR with two receiver channels having the same azimuth antenna pattern. This two-channel system may serve as an example for the unambiguous recovery of the Doppler spectrum resulting from a SAR signal recorded by the split antenna technique in TerraSAR-X [18] and Radarsat II [19]. Since it is possible to incorporate the transfer function due to the antenna pattern into the monostatic SAR response, the remaining difference between the two-channels is given by the two impulse responses

$$h_1(t;\Delta x_1) = \exp\left[-j\frac{\pi\Delta x_1^2}{2\lambda r_0}\right]\cdot\delta\left(t-\frac{\Delta x_1}{2v}\right) \quad \text{and} \quad h_2(t;\Delta x_2) = \exp\left[-j\frac{\pi\Delta x_2^2}{2\lambda r_0}\right]\cdot\delta\left(t-\frac{\Delta x_2}{2v}\right) \tag{7}$$

In the frequency domain, these impulse responses correspond to

$$H_1(f;\Delta x_1) = \exp\left[-j\frac{\pi\Delta x_1^2}{2\lambda r_0}\right]\cdot\exp\left(-j2\pi\frac{\Delta x_1}{2v}f\right) \quad \text{and} \quad H_2(f;\Delta x_2) = \exp\left[-j\frac{\pi\Delta x_2^2}{2\lambda r_0}\right]\cdot\exp\left(-j2\pi\frac{\Delta x_2}{2v}f\right) \tag{8}$$

The matrix $\mathbf{H(f)}$ is then given by

$$\mathbf{H(f)} = \begin{bmatrix} \exp\left[-j\pi\left(\frac{\Delta x_1^2}{2\lambda r_0}+\frac{\Delta x_1}{v}f\right)\right] & \exp\left[-j\pi\left(\frac{\Delta x_2^2}{2\lambda r_0}+\frac{\Delta x_2}{v}f\right)\right] \\ \exp\left[-j\pi\left(\frac{\Delta x_1^2}{2\lambda r_0}+\frac{\Delta x_1}{v}(f+PRF)\right)\right] & \exp\left[-j\pi\left(\frac{\Delta x_2^2}{2\lambda r_0}+\frac{\Delta x_2}{v}(f+PRF)\right)\right] \end{bmatrix} \tag{9}$$

and the inverse matrix $\mathbf{H^{-1}(f)}$ can be derived as

$$\mathbf{H^{-1}(f)} = \frac{1}{\exp\left(-j\pi\frac{\Delta x_2}{v}PRF\right)-\exp\left(-j\pi\frac{\Delta x_1}{v}PRF\right)}\begin{bmatrix} \exp\left[j\pi\left(\frac{\Delta x_1^2}{2\lambda r_0}+\frac{\Delta x_1}{v}f-\frac{\Delta x_2}{v}PRF\right)\right] & -\exp\left[j\pi\left(\frac{\Delta x_1^2}{2\lambda r_0}+\frac{\Delta x_1}{v}f\right)\right] \\ -\exp\left[j\pi\left(\frac{\Delta x_2^2}{2\lambda r_0}+\frac{\Delta x_2}{v}f-\frac{\Delta x_1}{v}PRF\right)\right] & \exp\left[j\pi\left(\frac{\Delta x_2^2}{2\lambda r_0}+\frac{\Delta x_2}{v}f\right)\right] \end{bmatrix} \tag{10}$$

The transfer functions of the reconstruction filters $P_1(f)$ and $P_2(f)$ are then given by

$$P_1(f) = \begin{cases} \dfrac{\exp\left(j\pi\Delta x_1^2/2\lambda r_0\right)\cdot\exp\left(j\pi\Delta x_1 f/v\right)}{1-\exp\left[j\pi\cdot PRF\cdot(\Delta x_2-\Delta x_1)/v\right]} & -PRF < f < 0 \\ \dfrac{\exp\left(j\pi\Delta x_1^2/2\lambda r_0\right)\cdot\exp\left(j\pi\Delta x_1 f/v\right)}{1-\exp\left[j\pi\cdot PRF\cdot(\Delta x_1-\Delta x_2)/v\right]} & 0 < f < PRF \end{cases} \tag{11}$$

and

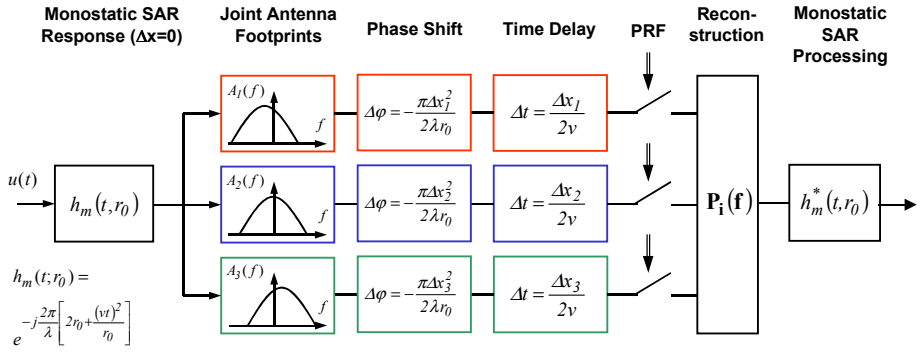

Figure 8: Quadratic phase approximation

$$P_2(f) = \begin{cases} \dfrac{\exp\left(j\pi\Delta x_2^2/2\lambda r_0\right)\cdot\exp\left(j\pi\Delta x_2 f/v\right)}{1-\exp\left[j\pi\cdot PRF\cdot\left(\Delta x_1-\Delta x_2\right)/v\right]} & -PRF < f < 0 \\ \dfrac{\exp\left(j\pi\Delta x_2^2/2\lambda r_0\right)\cdot\exp\left(j\pi\Delta x_2 f/v\right)}{1-\exp\left[j\pi\cdot PRF\cdot\left(\Delta x_2-\Delta x_1\right)/v\right]} & 0 < f < PRF \end{cases} \quad (12)$$

The numerator of the reconstruction filters can be regarded as compensating the different time delays and phase shifts within each branch, while the conjugate mirror structure in the denominator is responsible for a cancellation of the ambiguous frequencies within each branch. It becomes also clear that the denominator will vanish for $\Delta x_2 = \Delta x_1$ and a reconstruction becomes impossible due to the coinciding samples in azimuth.

Simulation example for three receivers:

As a simulation example, Figure 9 illustrates the results for a reconstruction of the non-ambiguous signal from a point target in case of a multistatic sparse aperture SAR with three receivers. In this simulation the three receivers have a non-optimum displacement and slightly different Doppler centroids. Furthermore, independent white noise has been added to each receiver channel in order to simulate a more realistic scenario. It becomes clear that the signal from each channel is strongly ambiguous while the coherent reconstruction of the three SAR signals will provide an efficient ambiguity suppression. The ambiguity suppression may also be regarded as a time-variant digital beamforming on receive where nulls in the joint antenna pattern are steered to the ambiguous areas (cf. [16][17]).

5. DISCUSSION

The performance of a bistatic SAR has been analyzed. The investigated system consists of a geostationary illuminator and multiple passive receivers in low earth orbits. Due to the long transmit path of a geostationary illuminator, the product of antenna size and transmit power has to be large for achieving a sufficient *NESZ* ($> 10^5 Wm^2$ in X-Band for a *NESZ* in the order of *–20dB* with small receivers). Forward scattering may increase the SNR for the investigated configuration by *10dB* and more [10][3], thereby substantially reducing the requirements on both the transmit power and antenna size. However, the current bandwidth limitation of *300MHz* in X-Band allows only a partial exploitation of forward scattering if high resolution imaging is required. Note that range resolution may also be improved by super-resolution techniques based on multiple receivers in appropriate orbits. The coverage region of a geostationary illuminator is restricted to approximately ±55° latitude due to the shallow incident angle with respect to the illuminator [3]. This restriction may be avoided by use of illuminators in geosynchronous orbits or in medium earth orbits. The phase noise of current oscillator technology will allow coherent integration times on the order of *10s* for an integrated sidelobe ratio (ISLR) of *–20dB* [3]. Limitations arise from the small footprints of the receiver antennas. These restrictions may be overcome by using digital beamforming on receive. Digital beamforming on receive has also the potential to improve both the radiometric and geometric resolution since it makes efficient use of the total signal power in the large illuminated footprint. Furthermore, ambiguity suppression by null-steering will enable the mapping of a wide image swath with compact SAR sensors and the data rate in digital beamforming can be reduced by an appropriate sub-sampling and/or time variant bit allocation.

Multistatic satellite constellations may allow for a suppression of azimuth ambiguities and therefore the aperture size of each individual receiver can be reduced. An appropriate algorithm for the suppression of azimuth ambiguities has been derived. This reconstruction algorithm, which is based on a coherent combination of the individual receiver signals, enables a recovery of the unambiguous SAR signal also in case of non-optimum receiver displacements leading to a non-uniform sampling of the synthetic aperture. This algorithm has also a great potential for systems relying on the displaced phase center (DPC) technique [12], like the Quad Array SAR [13], the high resolution wide swath (HRWS) SAR [14], as well as the split antenna approach in TerraSAR-X [18] and Radarsat II [19].

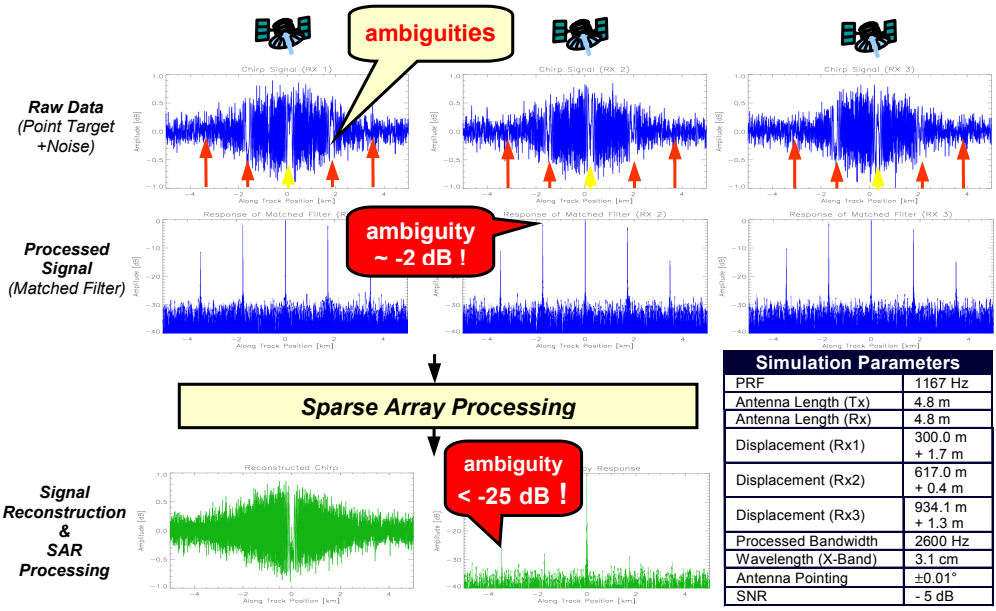

Simulation Parameters	
PRF	1167 Hz
Antenna Length (Tx)	4.8 m
Antenna Length (Rx)	4.8 m
Displacement (Rx1)	300.0 m + 1.7 m
Displacement (Rx2)	617.0 m + 0.4 m
Displacement (Rx3)	934.1 m + 1.3 m
Processed Bandwidth	2600 Hz
Wavelength (X-Band)	3.1 cm
Antenna Pointing	±0.01°
SNR	- 5 dB

Figure 9: Reconstruction from non-uniform sampling of sparse receiver apertures

A cross-track separation of the receivers will introduce an additional phase in the received signals, which has to be compensated, e.g., via the simultaneous acquisition of a digital elevation model in case of multiple satellites. The processing of these data will lead to a combination of cross-track interferometry and digital beamforming with sparse arrays. Since cross-track interferometry may be regarded as a second-order nonlinear filter, the combined operation of cross-track interferometry and linear ambiguity suppression may also be treated in the context of polynomial filters, which result from a Volterra series expansion of nonlinear functionals. A coherent processing of multiple receiver signals will require precise phase synchronization between the radar systems. This can be achieved either by means of ultra-stable oscillators or microwave links. Additional requirements are the accurate knowledge of the relative orbit position, satellite formation flight, lightweight antenna technology and efficient image formation algorithms. The solution of these challenges will lead to cost-effective SAR missions with reconfigurable satellite constellations for a broad range of powerful remote sensing applications. A first step in this direction is a bistatic airborne SAR experiment which has been performed in a close co-operation between ONERA and DLR.

6. REFERENCES

[1] K. Tomiyasu, "Bistatic Synthetic Aperture Radar using Two Satellites", IEEE EASCON, pp.106-110, 1978.
[2] P. Hartl and H.M. Braun, "A Bistatic Parasitical Radar (BIPAR), Proc. ISPRS, Kyoto, 1988.
[3] G. Krieger, H. Fiedler et al., "Bi- and Multistatic SAR Systems", SAFARI-TN-DLR-HR-4000, DLR Internal Report, Nov. 2002.
[4] G. Krieger, H.Fiedler, D. Hounam, and A. Moreira, "Analysis of System Concepts for Bi- and Multistatic SAR Missions", IGARSS 2003.
[5] D. Massonnet, "Capabilities and Limitations of the Interferometric Cartwheel", IEEE Trans. Geosci. Remote Sensing, Vol. 39(3), pp. 506-520, 2001.
[6] M. Martin, P. Klupar, S. Kilberg, J. Winter, "TechSat 21 and Revolutionizing Space Missions Using Microsatellites", American Institute of Aeronautics and Astronautics, 2001.
[7] A. Moccia, N. Chiacchio, A. Capone, "Spaceborne bistatic synthetic aperture radar for remote sensing applications", Int. J. Remote Sens. 21(18), pp. 3395-3414, 2000.
[8] N.B. Evans, P. Lee, R. Girard, "The Radarsat 2&3 Topographic Mission: An Overview", IGARSS 2002.
[9] G. Krieger, H. Fiedler, J. Mittermayer, K. Papathanassiou and A. Moreira, "Analysis of multistatic configurations for spaceborne SAR interferometry", IEE Proceedings - Radar Sonar Navigation 150 (3) , pp. 87- 96, 2003.
[10] N. Willis, "Bistatic Radar", Artech House, Boston, 1991.
[11] G. Krieger and A. Moreira, "Potentials of Digital Beamforming in Bi- and Multistatic SAR", IGARSS 2003.
[12] A. Currie and M.A. Brown, "Wide-Swath SAR", IEE Proceedings - Radar Sonar and Navigation 139 (2), pp 122-135, 1992.
[13] G.D. Callaghan and I.D. Longstaff, "Wide Swath Spaceborne SAR Using a Quad Element Array", IEE Radar Sonar and Navigation 146(3), pp 159-165, 1999.
[14] M. Suess, B. Grafmüller, R. Zahn, "A Novel High Resolution, Wide Swath SAR System", IGARSS 2001.
[15] M. Younis, C. Fischer, W. Wiesbeck, "An Evaluation of Performance Parameters of Reconfigurable SAR Systems", IGARSS 2002.
[16] N.A. Goodman, S.C. Lin, D. Rajakrishna, J.M. Stiles, "Processing of Multiple-Receiver Spaceborne Arrays for Wide Area SAR", IEEE Trans. Geosci. Remote Sensing 40 (4), pp 841-852, 2002.
[17] J.P. Aguttes, "The SAR Train Concept: Required Antenna Area Distributed over N Smaller Satellites, Increase of performance by N", IGARSS 2003.
[18] J. Mittermayer, H. Runge, "Conceptual Studies for Exploiting the TerraSAR-X Dual Receiving Antenna", IGARSS 2003.
[19] L. Brule, H. Baeggli, "Radarsat-2 Program Update", IGARSS 2002.
[20] A. Papoulis, "Generalized Sampling Expansion", IEEE Transactions on Circuits and Systems 24 (11) , pp.652-654, 1977.
[21] J.L. Brown, "Multi-Channel Sampling of Low-Pass Signals", IEEE Transactions on Circuits and Systems 28 (2) , pp.101-106, 1981.